Published in final edited form as:

*Nat Methods*. 2014 July ; 11(7): 749–755. doi:10.1038/nmeth.2992.

# Single-cell western blotting

**Alex J. Hughes**[1,2,6,7], **Dawn P. Spelke**[1,2,3,7], **Zhuchen Xu**[1,2], **Chi-Chih Kang**[1,2], **David V. Schaffer**[1,2,3,4,5], and **Amy E. Herr**[1,2,3]

[1]Department of Bioengineering, University of California, Berkeley (UC Berkeley), California, USA

[2]California Institute for Quantitative Biosciences, UC Berkeley, Berkeley, California, USA

[3]The UC Berkeley-UC San Francisco Graduate Program in Bioengineering, UC Berkeley, Berkeley, California, USA

[4]Department of Chemical Engineering, UC Berkeley, Berkeley, California, USA

[5]Helen Wills Neuroscience Institute, UC Berkeley, Berkeley, California, USA

## Abstract

To measure cell-to-cell variation in protein-mediated functions — a hallmark of biological processes — we developed an approach to conduct ~$10^3$ concurrent single-cell western blots (scWesterns) in ~4 hours. A microscope slide supporting a 30 μm-thick photoactive polyacrylamide gel enables western blotting comprised of: settling of single cells into microwells, lysis *in situ*, gel electrophoresis, photoinitiated blotting to immobilize proteins, and antibody probing. We apply this scWestern to monitor single rat neural stem cell differentiation and responses to mitogen stimulation. The scWestern quantifies target proteins even with off-target antibody binding, multiplexes to 11 protein targets per single cell with detection thresholds of <30,000 molecules, and supports analyses of low starting cell numbers (~200) when integrated with fluorescence activated cell sorting. The scWestern thus overcomes limitations in single-cell protein analysis (i.e., antibody fidelity, sensitivity, and starting cell number) and constitutes a versatile tool for the study of complex cell populations at single-cell resolution.



Correspondence should be addressed to D.V.S (schaffer@berkeley.edu) or A.E.H. (aeh@berkeley.edu).

[6]Present address: Department of Pharmaceutical Chemistry, UC San Francisco, San Francisco, California, USA.

[7]These authors contributed equally to this work.

**AUTHOR CONTRIBUTIONS**

A.J.H. and A.E.H. designed the scWestern. A.J.H., A.E.H., D.P.S., and D.V.S. designed experiments. A.J.H., Z.X., and C.-C. K. performed scWesterns and calibration experiments. D.P.S. performed NSC culture, stimulation and differentiation; conventional western blots, flow cytometry, and plate-based immunocytochemistry. A.J.H. and D.P.S performed in-microwell immunocytochemistry. A.J.H., D.P.S., and Z.X. performed confocal microscopy. Z.X. and A.J.H. designed software and performed analysis for cell/microwell scoring, immunoprobing quality control, and fluorescence quantitation. Z.X. performed fluid dynamics simulations. Validation data were analyzed by A.J.H, D.P.S., and Z.X. All authors wrote the manuscript.

**COMPETING INTERESTS STATEMENT**

A.J.H., Z.X., C.-C.K., and A.E.H. are inventors on pending patents related to scWestern blot methods. A.E.H. holds equity interest in Zephyrus Biosciences.

## INTRODUCTION

Heterogeneity is inherent in cellular processes including stem cell differentiation[1,2], development[3], cancer[4,5], pharmaceutical efficacy[6], and immune response[7]. Owing in large part to technological advances, genomic and transcriptomic studies of cell-to-cell heterogeneity are flourishing[4,8]. However, recent single-cell and population-wide studies comparing transcriptomes to proteomes in microorganismal and mammalian cells found only mild correlations between mRNA and protein expression[9–11]. Therefore, to fully understand diverse and often rare behaviors in complex cell populations, analytical tools are needed that are optimized for protein analysis of many cells, offer single-cell resolution, provide quantitative and highly specific detection of target proteins, and do not employ labels that may perturb protein and cell function[12].

Single-cell proteome-wide studies are currently limited to readouts from synthetic fluorescent protein fusion libraries[9,11], which while illuminating, are challenging to generate and can potentially perturb protein function. Single-cell protein immunoassays have proved immensely important for assessing cell-to-cell heterogeneity (e.g., flow cytometry[7]; immunocytochemistry, ICC[13]), yet existing methods depend on analyte discrimination with antibody probes that often have limited specificity. This dependence on antibody probe quality limits assay performance, as cross-reactivity can create misleading background signals that are difficult to correct for[14–16], even with careful controls[17,18]. This vulnerability broadly impacts antibody-based assays (e.g., enzyme-linked immunosorbent assays, ELISAs; protein microarrays[14]). To overcome limitations in antibody performance, the widely-used western blot first separates proteins by molecular mass (via electrophoresis) prior to the antibody probing step, thereby enabling clear discrimination between on-target and off-target signals, even in complex backgrounds such as cell lysates[19,20]. Nevertheless, the cell population averaging required by existing blotting tools masks the rich single-cell behaviors found in complex populations[20,21].

We address the need for high-specificity protein assays capable of measuring cell-to-cell heterogeneity within complex populations of cells by introducing a single-cell western blot (scWestern) in which ~2,000 individual cells are simultaneously assayed in <4 hours. We apply the scWestern to study variability in stem cell signaling and differentiation responses to homogeneous *in vitro* stimuli.

## RESULTS

### Characterization of scWesterns for single-cell analyses

scWestern analysis employs a microscope slide coated with a thin photoactive polyacrylamide (PA) gel[21] micropatterned with an array of 6,720 microwells (Fig. 1). The microwells (20 μm diameter) are patterned during polymerization of a 30 μm-thick PA gel against a silicon wafer studded with SU-8 microposts (Fig. 1a). To allow for concurrent western analysis of thousands of single cells, the scWestern integrates all key western blotting steps (Fig. 1b,c) in a dense array format.

Three fundamental design principles underpin the scWestern. Firstly, we address the scWestern globally in terms of fluidic, optical, and electrical interfacing. Global interfacing yields highly parallel analyses by eliminating independent hardware access to each of the thousands of microwells. Initially, a cell suspension is seeded into microwells via passive gravity-driven cell settling, resulting in capture of 0–4 cells/microwell in 5–10 min. For neural stem cell (NSC) densities of 1,000–1,800 cells/mm$^2$ slide area (2–3.5×10$^6$ cells in total), we observed single cells in 40–50% of microwells (Supplementary Fig. 1). Importantly, fluorescence-activated cell sorting (FACS) can be integrated with scWesterns to analyze subpopulations of ~200 cells with single-cell resolution (Supplementary Fig. 2), enabling analyses of rare or precious cells. Next, we buffer exchange to a denaturing RIPA buffer that lyses cells in the microwells in 2.6 ± 1.5 s (± S.D., $n$ = 6 cells, Supplementary Video 1), solubilizing intracellular proteins while providing a suitable conductivity for subsequent electrophoresis. Protein diffusion from cells occurred within ~10 s of lysis (Fig. 1e). Simulations suggest that diffusion of cell contents from microwells is responsible for protein losses of 40.2 ± 3.6% observed during lysis buffer introduction (± S.D., $n$ = 3 microwells from 3 separate slides; Supplementary Note 1 Supplementary Fig. 3). Future innovation of microwell enclosure methods or the use of higher-viscosity lysis buffers may reduce these losses.

As a second design principle, we achieve a high-density scWestern array by optimizing for short separation-distance polyacrylamide gel electrophoresis (PAGE). To initiate electrophoresis after cell lysis, an electric field is applied across the submerged scWestern slide, electrophoresing proteins through the microwell walls and into the thin PA gel sheet. To characterize this process, we assayed a ladder of purified fluorescently-labeled proteins (27–132 kDa, Fig. 1d) that partition into microwells (Supplementary Note 2, Supplementary Fig. 4). Under our denaturing, non-reducing PAGE conditions, we (*i*) observed stacking of purified proteins during electromigration into the bulk PA gel, (*ii*) verified a log-linear relationship between protein molecular mass and migration distance in scWestern separations, as anticipated for SDS-PAGE[21,22] ($R^2$ = 0.97, Supplementary Fig. 5), and (*iii*) resolved covalent protein dimers (Supplementary Fig. 6). Moderate PAGE performance is achieved, with molecular mass differences of 51% ± 1.6% (± S.D., $n$ = 3 separations) resolvable in ~500 μm separation lengths and 30 s separation times. In general, we observe agreement between scWestern separations and conventional western blotting (see Supplementary Note 3). A recently described microwestern array (integrated with robotic bulk cell lysate printing) offers similar resolving power in 18-fold longer separation distances (9 mm)[20].

The third scWestern design principle harnesses small characteristic lengths for reaction (protein immobilization) and transport (antibody probing). Following PAGE, protein immobilization relies on a benzophenone methacrylamide co-monomer crosslinked into the PA gel. We measure protein photo-capture in the gel at 27.5% ± 2.9% of EGFP from EGFP-expressing NSCs after brief (45 s) gel exposure to UV light (± S.D., $n$ = 6 single cells from experiments on 4 separate days, Fig. 1e). Photo-immobilization benefits from small diffusion lengths between proteins and benzophenone moieties within the PA gel[21]. Probing of the separated, immobilized proteins is performed by sequential diffusion of primary and

secondary antibodies into the thin PA gel layer, taking advantage of the short 30 μm characteristic transport length (Supplementary Fig. 7 and 8; Supplementary Note 2). scWestern antibody consumption is comparable to conventional western blotting and ICC, with potential for additional optimization (Supplementary Note 2).

Analysis of multiple protein targets is crucial to understanding cell functions such as signal transduction[1]. Our scWesterns are organized into 16 assay "blocks" of 420 microwells each, a layout that allows application of different antibody solutions to different blocks. After probing, imaging with a fluorescence microarray scanner yields scWesterns of up to 48 targets per array (3-plex target quantitation for 16 microwell blocks). To further advance multiplexed analyte detection, we adopted serial stripping of antibodies using a strongly denaturing buffer. Using 11 antibody probe sets during nine stripping and re-probing rounds; nine unique targets were successfully detected in the same cell by scWestern blotting and validated by conventional western blotting (Supplementary Fig. 9 and 10). Stripping successfully removed antibody probes from scWestern slides, leading to >10-fold reductions in the signal-to-noise ratios (SNRs) compared to initial SNRs (Fig. 1e, Supplementary Fig. 11). Furthermore, reprobing after the first stripping round led to full recovery of initial probe signals, and signal recoveries of 50% were typical even after nine stripping and re-probing rounds (Supplementary Fig. 9b, Supplementary Fig. 11). Robust signal recovery is likely enabled by stable, covalent protein immobilization, in contrast to the relatively poor recovery observed in conventional platforms that utilize non-covalent blotting[23]. As a result, scWestern slides can be stored for long-term archiving and re-analysis of single-cell separations.

## Quantitative performance and calibration of scWesterns

We next sought to assay cellular signaling and differentiation in stem cells, which often exhibit diverse behaviors in response to homogeneous stimuli[1,2]. Initially, we applied the scWestern to NSCs transduced with a retroviral vector encoding EGFP using 12 blocks of a single slide (Fig. 2a). 4,128 separations of a possible 5,040 (82%) passed semi-automated gating on dust particles and gel defects. Additionally, 1,608 separations (39%) came from single cells, based on bright-field microwell occupancy determination (cells/microwell); and the microwell occupancy running average ranged between 0.0–2.1 cells/microwell with a mean of 1.1 cells/microwell (Fig. 2b). Automated occupancy scoring was used for all other data sets to identify single cell/microwell separations (**Online Methods**), and in all cases, large numbers of microwells housed single cells.

Two protein targets, EGFP and β-tubulin (βTUB), were probed on the same scWestern slide, and the resulting probed band intensities were correlated with microwell occupancy (Fig. 2a,b, Supplementary Fig. 12 and 13). We observed a monotonic but non-linear relationship between total fluorescence of the βTUB band and microwell occupancy (Fig. 2b), likely due to cell size-related bias for microwells with >1 cell (Supplementary Note 4). The βTUB fluorescence distribution for single-cell separations was well-described by a gamma distribution derived from a stochastic kinetic model of transcription and translation in a homogeneous population of dividing cells[24]. Our scWestern analysis of βTUB thus agrees

with gamma-distributed single-cell protein expression profiles reported for fluorescent protein fusion libraries in *E. coli*[9,25] and mammalian cells[26].

When benchmarked against flow cytometry, we observed 19% and 26.7% ± 1.1% of the NSCs to be EGFP+ (i.e., probed band signals above technical noise) by scWestern analysis and flow cytometry, respectively (± S.D., $n = 3$ technical replicates; Fig. 2c). The dynamic ranges were comparable (Supplementary Note 5).

To determine the linearity and sensitivity of scWestern fluorescence readouts, we undertook "direct" calibration of EGFP and "indirect" calibration of both EGFP and βTUB, as well as phosphorylated and total levels of the signaling protein ERK (Fig. 2d). Direct calibration correlates the number of purified EGFP molecules in a coverglass-enclosed microwell separation to probe fluorescence after immunoprobing, whereas the indirect method uses a partition coefficient measurement to infer the number of molecules in a dot-blotted scWestern band (Supplementary Note 6, Supplementary Fig. 14–16). The calibration results agree for EGFP (Fig. 2d) and, together with the indirect calibration data, suggest a linear dynamic range of 1.3–2.2 orders of magnitude, from a limit of detection of 45 zmol (27,000 molecules, comparable to fluorescence cytometry detection limits of $10^3$–$10^7$ molecules[27]). This detection limit matches an ideal noise threshold of 25,000 molecules set by the fluorescence microarray scanner to within 10%, is 45-fold more sensitive than microwestern arrays[20], and is 3.2-fold more sensitive than microfluidic western blotting[21] (Supplementary Note 5). For context, a median protein copy number of 50,000 has been reported for murine fibroblasts[10]; indicating that >50% of the mammalian proteome may be accessible via scWesterns (given the availability of suitable antibodies).

## Heterogeneity in signaling after FGF-2 stimulation of NSCs

A defining property of stem cells is self-renewal — or maintenance of an immature state[28]. Fibroblast growth factor-2 (FGF-2) is a mitogen and self-renewal signal for adult hippocampal NSCs[28,29], acting via the FGFR-1 receptor to activate the Ras-MAPK, p38 MAP, and PI3K-Akt pathways[29]. Signals are transmitted in MAPK cascades by sequential phosphorylation of downstream kinases, including MEK and ERK. scWesterns were applied to study MAPK signaling dynamics within single NSCs that were starved of FGF-2, suspended, settled into scWestern microwells, and stimulated with FGF-2 over a 60 min time course (Fig. 3). We first probed for phosphorylated ERK1/2 (pERK) and MEK1/2 (pMEK), followed by re-probing for total ERK1/2 and MEK1/2 (Fig. 3a, Supplementary Fig. 17). In parallel, βTUB and EGFP probing allowed estimation of molecular mass, and all targets were within 10% of their nominal masses.

scWestern analysis for pERK reported two proteins reactive to the anti-pERK antibody: the expected 38.8 ± 1.0 kDa protein, along with a heavier one of 103 ± 3 kDa (± S.D., $n = 3$ separations). We hypothesize that the 103 kDa protein arose from off-target antibody probing, since its pERK and ERK antibody fluorescence signals did not correspond (Fig. 3a). This off-target band may be ERK5 (~80–100 kDa), since ERK5 has high sequence homology with ERK1/2, and since pERK1/2 antibodies have been previously shown to cross-react with pERK5[30]. The off-target band for pERK exhibited considerable cell-to-cell variability, did not correlate with on-target pERK signal, and would have contributed up to

52% (with an average of 13%) of the overall pERK signal in unstimulated cells if not electrophoretically resolved from specific signal (Fig. 3b, Supplementary Fig. 18 and 19). Off-target probe binding can substantially influence existing single-cell immunofluorescence assays (e.g., ICC, flow cytometry), unless complex target-specific knock-down experiments are performed[16,17]. In contrast, scWestern analysis is intrinsically well-suited to identifying and discarding off-target probing signals.

Both scWesterns and conventional western blotting revealed dynamic, transient ERK and MEK phosphorylation responses (Fig. 3c–e, Supplementary Fig. 20), while the scWestern enabled analysis of statistical differences (Supplementary Note 7). Maximal pMEK:MEK phosphorylation levels agreed quantitatively, with ~3.5-fold increases compared to the zero time-point (for single-cell data, fold-change is relative to a mean fold-change of 1 at the zero time-points). A larger maximum fold-change in the pERK:ERK ratio was observed, consistent with signal amplification in the MAPK phosphorylation cascade[31].

We next compared scWesterns to a conventional single-cell technique — high-throughput ICC (Fig. 3f, Supplementary Fig. 21–24). pERK:ERK responses by ICC were similar to those measured by scWestern and conventional western assays, while pMEK:MEK responses by ICC were strongly attenuated with a maximum mean fold-change of <2 (Supplementary Note 7). We attribute the lower apparent response to non-specific signal from spurious nuclear localization of the pMEK antibody (a common artifact in ICC[16]), which obscures the subtle phosphorylation dynamics measurable by scWestern analysis.

Unlike conventional western blots, scWesterns quantified highly variable NSC responses to external stimuli. MEK was activated within 5 min in response to FGF-2, followed closely by ERK, as expected (Fig. 3e). However, a considerable spread in the MEK signal was observed, which was strongly amplified into a broad distribution in ERK activation at 12 min, followed by a transient decay in phosphorylation of both enzymes. This propagation of variation from MEK to ERK upon pathway activation is reflected in interquartile ranges of 3.7 and 7.3 fold-change units at 12 min for pMEK:MEK and pERK:ERK, respectively. The pERK:ERK distributions were skewed towards higher phosphorylation levels for the 0 and 60 min time-points due to the presence of rare activated cells (Fig. 3e, Supplementary Fig. 25). This rare activated state may arise from constitutive signaling or transient FGF-independent excursions from baseline phosphorylation states[32].

## Heterogeneity in NSC differentiation

In addition to self-renewal, a second hallmark of NSCs is multipotent differentiation from an immature state (markers SOX2+ and nestin, NEST+) into multiple lineages, such as astrocytes (glial fibrillary acidic protein, GFAP+) and neurons (βIII-tubulin, βIIITUB+)[13]. As with many stem cells, exposure of NSCs to uniform culture conditions can drive stochastic differentiation[13,32]. We applied the scWestern to study immature NSCs and their differentiation over a six-day period under mixed differentiation conditions that yielded both astrocytes and neurons (Fig. 4). Every 24 h, differentiating NSCs were settled into microwells (Fig. 4a–c) and analyzed. ICC in scWestern microwells did not suggest cell type or shape bias upon transfer of differentiated cells to microwells (Supplementary Table 1). The scWesterns successfully reported single bands for SOX2 (43.3 ± 1.9 kDa), βIIITUB

(47.2 ± 0.7 kDa), and GFAP (54.0 ± 1.0 kDa, ± S.D., *n* = 3 separations; Fig. 4d, Supplementary Fig. 26). Each target protein was within 30% of its expected mass (Supplementary Note 8).

NEST is an intermediate filament protein hypothesized to regulate structural dynamics and cytoplasmic trafficking within neural stem and progenitor cells undergoing rapid rounds of division[33]. Intermediate filament proteins often undergo regulation by alternative mRNA splicing, producing diverse isoforms that impact cell responses to stress and modulate intracellular signaling[34]. In agreement with literature reports[35,36], NEST exhibited low and high molecular mass bands by scWestern analysis that we denote NEST$^{\alpha}$ (95.7 ± 3.5 kDa, ± S.D., *n* = 3 separations) and NEST$^{\beta}$ (retained near the microwell edge) respectively (Fig. 4d, Supplementary Fig. 26). NEST$^{\beta}$ fully penetrated the scWestern gel for longer separation distances, indicating that this species is not an insoluble form of NEST (Supplementary Fig. 27).

We further scrutinized NEST$^{\alpha}$ and NEST$^{\beta}$ by conventional western and scWestern analysis with a second antibody (rat-401) against an epitope known to be excised by alternative splicing in a third 46 kDa isoform, Nes-S[37]. As for Nes-S, NEST$^{\alpha}$ was not detected by the rat-401 antibody (Supplementary Fig. 28), suggesting that NEST$^{\alpha}$ may be an alternatively spliced (or otherwise truncated) form of NEST$^{\beta}$ distinct from Nes-S. Intriguingly, NEST$^{\beta}$ was present at all time-points over the 6-day experiment, while NEST$^{\alpha}$ was variably expressed between cells and sharply down-regulated during differentiation. Indeed, contributions of NEST$^{\beta}$ unrelated to proliferative capacity may account for the apparent promiscuity in NEST expression observed in various mature neural cells by ICC (including in our data, Fig. 4a)[38]. NEST also exhibited two bands in conventional western blotting (114 and 270 kDa respectively, Fig. 4e, Supplementary Fig. 29), though the extensive cell-to-cell variation in NEST$^{\alpha}$ expression was not detectable with a conventional western.

Consistent with progressive conversion of NSCs to differentiated lineages, conventional western blotting confirmed >10-fold reductions in NEST$^{\alpha}$ (but not NEST$^{\beta}$) and SOX2, with accompanying >10-fold increases in βIIITUB and GFAP over the six-day period (Fig. 4e). Likewise, both culture plate and in-microwell ICC showed a corresponding reduction in total NEST+ NSCs, from ~90 to 40% of all cells. Similar overall trends were observed for scWestern data, normalized to constitutively expressed βTUB (Fig. 4f, Supplementary Fig. 30 and 31). On day six, scWesterns put the fractions of committed βIIITUB+ neurons and GFAP+ astrocytes at 53% and 7.1% respectively, matching ICC to within 15% (Supplementary Table 1).

Importantly, scWesterns revealed high cell-to-cell marker expression variability, including profound increases in GFAP expression in the relatively rare astrocyte population over the course of differentiation, spanning a range of 46-fold on day six. Single-cell expression levels of NEST$^{\alpha}$ at day 0 spanned a range of 22-fold relative to its technical noise threshold, and the proportion of cells expressing NEST$^{\alpha}$ dropped from 53 to 2% between days 0 and 6.

Additionally, scWestern blots successfully resolved off-target antibody signal of approximately equal magnitude to specific signal for MASH1 (ASCL1, a 34 kDa

transcription factor involved in neuronal fate commitment) in late-passage, undifferentiated NSCs, as corroborated by conventional western blot (Supplementary Fig. 32). These data confirm the ability of scWestern assays to accurately capture population expression dynamics by combining the single-cell capabilities of ICC with the molecular mass specificity of conventional western blotting.

## DISCUSSION

We demonstrate a single-cell protein analysis technique capable of quantitative, multiplexed, and at-the-bench operation as an avenue to advance our understanding of cell-to-cell variation in protein-mediated cell functions. Importantly, given the often mediocre performance of antibodies as probes[16,39], advances in assay specificity are necessary to discriminate between legitimate and spurious protein signals. Western blotting offers high protein specificity, as the technique reports both target molecular mass (via protein electrophoresis) and probe binding (via subsequent antibody probing); not simply probe binding[18]. scWesterns bring this specificity to the analysis of single cells, pointing towards a rich, graded heterogeneity in stem cell signaling trajectories. Furthermore, by reporting molecular mass as well as antibody binding, the scWestern identifies two putative nestin isoforms and suggests that one ($NEST^{\alpha}$), better reflects exit of NSCs from the immature state. In contrast, antibody binding assays (ICC, flow cytometry) struggle to distinguish such isoforms. Clonal lineage tracing — aided by scWestern analyses — may enable further mechanistic insights into the functions of NEST isoforms[26].

More broadly, we envision a role for scWesterns in applications that integrate upstream functional or morphological screens, quantify cell-to-cell response to pharmaceutical agents (including rare circulating tumor cells[5]), and advance affinity reagent performance by easing library screens.

## ONLINE METHODS

### Cell culture

Neural stem cells (NSCs) were isolated from the hippocampi of adult female Fisher 344 rats[28] and cultured on tissue culture-treated polystyrene plates coated with 10 μg/mL polyornithine (P3655, Sigma-Aldrich) and 5 μg/mL laminin (23017-015, Life Technologies). NSCs were found to be mycoplasma-free within 12 months both prior to and following use in experiments. NSCs were cultured in 1:1 DMEM-F12 (11039-021, Life Technologies) supplemented with N-2 (17502-048, Life Technologies) and 20 ng/mL recombinant human FGF-2 (100-18, PeproTech), and subcultured at 80% confluency using Accutase (A11105-01, Life Technologies) for cell detachment.

EGFP NSC cell lines were created through stable retroviral infection. The retroviral vector pCLPIT-GFP[41] was packaged[42] and purified virus was titered on NPCs. High-expressing EGFP NSCs were infected at a multiplicity of infection of 3 (MOI = 3) and analyzed in Fig. 2, while low expressing EGFP NSCs were infected at MOI = 0.5 and used in all other studies. Stable cell lines were obtained through selection in media containing 0.3 μg/ml puromycin for 72 h (P8833, Sigma-Aldrich).

EGFP NSCs for scWestern EGFP expression studies were cultured as described for uninfected NSCs. For scWestern signaling studies, EGFP NSCs were FGF-starved for 16 hours. Cells were detached with accutase and suspensions analyzed by scWesterns (see **scWestern**.). EGFP NSCs for scWestern differentiation studies were cultured in DMEM-F12-N2 supplemented with 0.5 ng/mL FGF-2, 1 μM retinoic acid (RA, BML-GR100, Enzo Life Sciences), and 1% fetal bovine serum (FBS, SH3008803, ThermoFisher Scientific) for 0–6 days. Cells were detached with trypsin EDTA after the desired differentiation time (25-053-Cl, Corning Cellgro) and analyzed (N.B. cells were not differentiated within microwells; see **scWestern**).

## Proteins and reagents

15 μm fluorescent polystyrene microspheres were from Life Technologies (F-8844). Alexa Fluor 488-labeled purified ovalbumin and bovine serum albumin were also from Life Technologies (O34781, A13100). Purified standards for scWestern calibration were: β-tubulin from bovine brain (TL238, Cytoskeleton), recombinant EGFP, His-tagged (4999-100, BioVision), recombinant human pERK1 (ab116536, Abcam). Aliquots of these purified standards were labeled with Alexa Fluor 568 using a protein labeling kit according to vendor instructions (A-10238, Life Technologies) for the determination of partition coefficients in indirect calibration experiments (see **scWestern calibration**.).

Purified His-tagged dronpa was expressed in Rosetta competent cells transformed using a pET His6 tobacco etch virus (TEV) ligase independent cloning (LIC) vector, 2BT (EMD Millipore), grown in 2YT medium at 37°C to an OD600 of 0.5, induced with 0.5 mM IPTG and grown for an additional 2.5 hours at 37°C before harvesting. Cells were pelleted by centrifugation at 5,000 rpm for 15 mins at 4°C and the pellets resuspended in Nickel buffer A supplemented with protease inhibitors (25 mM HEPES pH 7.5, 400 mM NaCl, 10% glycerol, 20 mM imidazole, 1 μg/ml leupeptin and pepstatin, 0.5 mM PMSF). Cells were lysed using an Avestin C3 homogenizer at a pressure of 15,000 psi. Cell debris was pelleted at 15,000 rpm for 30 min. The clarified lysate was loaded onto a 5 ml HisTrap FF Crude column (GE Healthcare), and unbound material was washed out with Nickel buffer A. Bound protein was eluted with a 10CV gradient up to 400 mM imidazole in Nickel buffer A. Absorption of the eluting material was monitored at 503 nm as well as at 280 nm to aid in pooling the target protein. Fractions containing dronpa were pooled and desalted into IEX buffer A (50 mM sodium phosphate pH 6.5). Desalted protein was loaded onto a 5 ml SP HP ion exchange column (GE Healthcare) and unbound material was washed out with IEX buffer A. Bound material was eluted with a 20CV gradient up to 1 M NaCl in IEX buffer A. Fractions containing dronpa were pooled and assayed for aggregation by analytical size exclusion chromatography on a Superdex 200 5/150 column (GE Healthcare) equilibrated in 25 mM HEPES, 400 mM NaCl, 10% glycerol, 1 mM DTT. Samples were finally desalted into storage buffer (50 mM sodium phosphate pH 6.5, 150 mM NaCl, 10% glycerol, 1 mM DTT).

Details of antibody reagents used are listed in the methods sections corresponding to scWestern, conventional western blotting, and immunocytochemistry assays.

N-[3-[(4-benzoylphenyl)formamido]propyl] methacrylamide (BPMAC) was synthesized in-house via the reaction of the succinimidyl ester of 4-benzoylbenzoic acid with *N*-(3-aminopropyl)methacrylamide hydrochloride in the presence of catalytic triethylamine according to standard protocols[21,43].

### Fabrication of microwell scWestern substrates

SU-8 microposts were fabricated on mechanical grade silicon wafers by standard soft lithography methods. SU-8 2025 photoresist (Y111069, MicroChem) was spun to a thickness of (typically) 30 μm according to manufacturer guidelines and exposed to 365 nm UV light at ~40 mW/cm$^2$ for 12 s under a mylar mask printed with 20 μm circular features at 20,000 dpi (CAD/Art Services). The features were arranged in a square configuration with a pitch of 500 μm in the direction of separations and 190 μm in the transverse direction (a pitch of 700 μm yielded separation lengths sufficient for NEST$^\beta$ to fully enter the scWestern gel). 2×8 blocks of 14×30 features (6,720 total) were spaced 9 mm apart to match the dimensions of a 2×8 well microarray hybridization cassette (AHC1X16, ArrayIt). 1 mm-thick rails spanning the length of the micropost array at a spacing of 24 mm were also patterned to support glass substrates at the height of the microposts. Uniformity of features was verified by optical profilometry after exposure and development using SU-8 developer solution (Y020100, MicroChem). The measured feature heights and diameters within a micropost block were 30.30 ± 0.15 μm (± S.D., $n$ = 4 microposts) and 20.52 ± 0.68 μm (± S.D., $n$ = 4 microposts) for respective nominal dimensions of 30 μm and 20 μm. Between-block CV's in the height and diameter measurements for blocks spaced across the full length of the array were 1.1% and 5.2%, respectively ($n$ = 3 microposts). Wafers were silanized by vapor-deposition of 2 ml of the hydrophobic silane dichlorodimethylsilane (DCDMS, 440272, Sigma-Aldrich) for 1 hour *in vacuo*, washed thoroughly with deionized (DI) water, and dried under a nitrogen stream immediately prior to use. Silanized wafers were robust to reuse after rinsing with DI water in excess of 20 times with moderate delamination of micropost structures.

Plain glass microscope slides (48300-047, VWR) were silanized to establish a self-assembled surface monolayer of methacrylate functional groups according to standard protocols[44]. Silanized slides were placed face-down onto micropost wafers and manually aligned to the SU-8 rail and micropost features. Gel precursor solutions were 8%T (wt/vol total acrylamides), 2.7%C (wt/wt of the crosslinker N,N'-methylenebisacrylamide) from a 30%T, 2.7%C stock (A3699, Sigma-Aldrich); 3 mM BPMAC from a 100 mM stock in DMSO, 0.1% SDS (161-0301, BioRad), 0.1% Triton X-100 (BP151, Fisher), 0.0006% riboflavin 5' phosphate (F1392, Sigma-Aldrich), 0.015% ammonium persulfate (APS, A3678, Sigma-Aldrich), and 0.05% tetramethylethylenediamine (TEMED, T9281, Sigma-Aldrich) in 75 mM tris buffer titrated with HCl to a p*H* of 8.8. For confocal imaging of cells in rhodamine-tagged scWestern gels, the precursor included the fluorescent monomer methacryloxyethyl thiocarbamoyl rhodamine B (23591, Polysciences) at 3 μM from a 100 μM stock in DMSO. The precursor mixture was sonicated and degassed (Aquasonic 50D, VWR) for 1 min *in vacuo* immediately prior to the addition of detergents (SDS, Triton) and polymerization initiators (riboflavin, APS, TEMED). The precursor was then injected into the gap between the glass slide and silicon wafer using a standard 200 μl pipet. After

allowing ~30 s for precursor to wick through the gap, the slide was exposed to blue light for 7.5 min at 470 lux (advanced light meter, 840022, Sper Scientific) from a collimated 470 nm LED (M470L2-C1, Thor Labs) mounted at a 45° angle above the slide. Polymerization was allowed to continue for an additional 11 min. Gel-fabricated glass slides were wetted at their edges using 2 ml of phosphate-buffered saline (PBS), pH 7.4 (21-040, Corning) and carefully levered from wafers using a razor blade. Fabricated slides could be stored at 4°C in PBS for up to 2 weeks before use without loss of protein separation or photocapture properties.

### scWestern

Fabricated slides were removed from PBS and excess liquid drained to a corner by gravity and absorbed using a kimwipe (Kimberly-Clark). 1–2 ml of cell suspension was applied evenly across the surface of the slide and allowed to settle on a flat surface within a 100×100 mm petri dish. Settling times varied from 5–30 min, with microwell occupancy monitored by brightfield microscopy until single-cell occupancies of roughly 40–50% were achieved. Intermittent, gentle movement of the petri dish every 2–5 min for 10 s was sufficient to ensure cell access to microwells through cell rolling on the gel surface. After settling, slides were lifted to a 10–20° angle from one of the short edges to remove excess cell media, and cells on the surface of the slide were removed by gentle pipetting of 4–5 1 ml aliquots of PBS to the raised edge of the slide surface, with excess buffer removed from the lower edge by vacuum. Slides were placed flat and prepared for cell counting by applying 1 ml of PBS onto the slide. A second plain glass slide was applied to the PBS layer from one short edge to the other to prevent entrapment of bubbles, and lowered to form a “sandwich” of slides. Microwells within the sandwich were imaged by brightfield microscopy at 4× magnification (Olympus UPlanFLN NA 0.13) using 50 ms exposure times at 1×1 pixel binning and a preset position list to guide a mechanical stage (Olympus IX71 inverted fluorescence microscope equipped with iXon+ EMCCD camera, Andor; motorized stage, ASI; and shuttered mercury lamp light source, X-cite, Lumen Dynamics; controlled by MetaMorph software, Molecular Devices). All 6,720 features could be imaged in ~4 min.

After cell counting, the top glass slide was removed from the sandwich by sliding gently across the gel layer. The scWestern slide with settled cells was then immediately transferred to a custom 60×100 mm horizontal electrophoresis chamber fabricated from 3 mm-thick perspex plastic. Platinum wire electrodes (0.5 mm diameter, 267228, Sigma-Aldrich) were placed along the long edge of the chamber and interfaced with alligator clips to a standard electrophoresis power supply (Model 250/2.5, BioRad). Slides were temporarily adhered to the bottom face of the chamber using petroleum jelly. 10 ml of a denaturing RIPA lysis/electrophoresis buffer consisting of 0.5% SDS, 0.1% v/v Triton X-100, 0.25% sodium deoxycholate (D6750, Sigma-Aldrich) in 12.5 mM tris, 96 mM glycine pH 8.3 (0.5× from a 10× stock, 161-0734, BioRad) was poured over the slide to lyse cells. This buffer was supplemented with 1 mM sodium fluoride and sodium orthovanadate for phosphoprotein analyses (S7920 and 450243, Sigma-Aldrich). The RIPA buffer provides denaturing but non-reducing conditions, since reduction typically requires heating in the presence of a reducing agent for timescales longer than protein diffusion from microwells[21]. Lysis proceeded for 10 s with electric field off, followed by application of 200V ($E$ = 40 V/cm) for

~30 s. Separations from single EGFP-expressing NSCs were monitored in real time at 10× magnification (UPlanFLN NA 0.3 objective) using a filter set optimized for EGFP (XF100-3, Omega Optical), 4×4 camera binning, 250 ms exposure time. Following separations, slides were immediately exposed for 45 s from above using a UV mercury arc lamp (Lightningcure LC5, Hamamatsu) directed through a Lumatec series 380 liquid light guide with inline UV filter (300–380 nm bandpass, XF1001, Omega Optical) suspended approximately 10 cm above the slide with UV power at the slide surface of ~40 mW/cm$^2$ (320–400 nm UV meter; C6080-365, Hamamatsu).

Following separation and photocapture of cell contents, slides were washed using 10 ml of the denaturing RIPA buffer, followed by 10 ml of TBST (100 mM tris titrated to pH 7.5 with HCl, 150 mM NaCl, 0.1% Tween 20, 9480, EMD Millipore), each for 10 min. Slides could be stored prior to successful immunoprobing for at least 1 wk at 4°C in TBST.

In FGF-2 stimulation experiments, cells were stimulated between cell/microwell counting and lysis/electrophoresis steps by applying 1 ml of 20 ng/ml FGF-spiked culture media to the slide surface for the desired stimulation time.

### Purified protein scWesterns

Purified proteins were assayed using a similar protocol to that for single cells. Gel slides were incubated with purified proteins in denaturing RIPA buffer for 30 min, submerged in fresh denaturing RIPA for 5 s, and "sandwiched" with a second glass slide to trap proteins within the gel layer. The glass slide sandwich was subjected to electrophoresis, UV-mediated protein capture, washing, and probing as in single-cell assays; the top glass layer was removed after the capture step.

### scWestern probing, imaging, and stripping

Slides were probed with primary and fluorescently labeled secondary antibodies by diffusive delivery in 2×8 well microarray hybridization cassettes (AHC1X16, ArrayIt).

Primary antibodies with fold-dilutions employed for single-cell, purified protein, and calibration assays (unless otherwise noted) were: rabbit anti-ovalbumin (1:20, ab1221, Abcam), goat anti-GFP (1:20, ab6673, Abcam), rabbit anti-β-tubulin (1:20, ab6046, Abcam), rabbit anti-pERK1/2 (1:40, Thr202/Tyr204, 4370, Cell Signaling), rabbit anti-ERK1/2 (1:20, 4695, Cell Signaling), mouse anti-ERK1/2 ("ERK # 2", 1:20, 4696, Cell Signaling), rabbit anti-pMEK1/2 (1:40, Ser217/Ser221, 9154, Cell Signaling), rabbit anti-MEK1/2 (1:20, 9126, Cell Signaling), goat anti-SOX2 (1:20, sc-17320, Santa Cruz Biotechnology), mouse anti-nestin ("NEST", 1:20, 611658, BD Biosciences), mouse anti-nestin ("NEST #2", 1:20, MAB353, clone: rat-401, EMD Millipore), goat anti-EphB4 (1:20, AF446, R&D Systems), mouse anti-MASH1 (1:20, 556604, BD Biosciences), mouse anti-SRC (1:20, 05-184, EMD Millipore), goat anti-GFAP (1:20, ab53554, Abcam), mouse anti-βIII-tubulin (1:20, T8578, Sigma-Aldrich). Secondary antibodies were Alexa Fluor 488-, 555-, or 647-labeled donkey anti-mouse, rabbit, or goat IgG from Life Technologies (A31571, A31573, A21447, A31570, A31572, A21432, A21202, A21206, A11055), except for the probing of ovalbumin in Supplementary Fig. 7, which used Alexa Fluor 568-labeled

goat anti-rabbit IgG (A-11011, Life Technologies). All were used at the same dilution factor as the corresponding primary antibody.

Each block of separations was incubated at room temperature with 40 μl of primary antibody solution diluted in TBST supplemented with 2% bovine serum albumin (BSA, A730, Sigma-Aldrich) for 1 hour under gentle orbital shaking. Slides were removed from hybridization cassettes and washed 3 times in 10 ml TBST for 15 min per wash (45 min total), also under gentle orbital shaking. Slides were then similarly probed and washed with fluorescently labeled secondary antibodies in TBST supplemented with 2% BSA. Slides were washed a final time in 10 ml DI water for 5 min and dried under a nitrogen stream. Imaging was conducted using a GenePix 4300A microarray scanner with PMT gains of 400–550 and laser powers of 30–100%, optimized for maximum dynamic range without saturation of target band fluorescence values. Filter sets were employed for 3-channel detection using Alexa Fluor 488, 555, and 647-labeled secondary antibodies using 488, 532, and 635 nm lasers, respectively. 12.5 mm diameter emission filters for the 488 and 532 nm spectral channels were from Omega Optical (XF3405 and XF3403, respectively); the 635 nm channel employed a built-in far-red emission filter.

Spectral bleed-through was below noise thresholds of on-target fluorescence line profiles, except for co-probing of ERK or β-tubulin (Alexa Fluor 555-labeled secondary antibody) with EGFP (Alexa Fluor 488-labeled secondary antibody) in Figs. 3 and 4 respectively. Ratio metrics in Fig. 3d,e for which ERK bands were affected by EGFP bleed-through above technical noise were discarded from analysis. Ratio metrics in Fig. 4f derived from β-tubulin bands similarly affected by EGFP bleed-through were also discarded. No fluorescence micrographs or derived data sets were fluorescence-compensated for spectral bleed-through.

Stripping of slides was performed via 3 hour incubations in a stripping buffer heated to 50°C consisting of 2.5% SDS and 1% β-mercaptoethanol (M3148, Sigma-Aldrich) in 62.5 mM tris titrated to pH 6.8 with HCl. Following stripping, slides were washed 3 times in 10 ml aliquots of TBST for 5 min per wash and stored in TBST at 4°C until re-probing. For longer-term archiving, stripped, air-dried slides could be successfully reprobed after extended (>1 month) storage at 4°C.

## scWestern data analysis

Cell/microwell scoring was conducted manually or via custom software designed in-house that employed scripts to mate thresholding and particle analysis on the basis of cell size and circularity in ImageJ (http://rsbweb.nih.gov/ij/) to downstream gating to identify microwells containing single cells in R (http://www.r-project.org), see (Supplementary Software).

To quantify the performance of automated cell/microwell scoring, we calculated precision = $tp/(tp+fp)$ and sensitivity = $tp/(tp + fn)$, where $tp$ is the number of microwells scored as containing single cells that actually contained single cells, $fp$ is the number of microwells scored as containing single cells that did not contain single cells, and $fn$ is the number of microwells scored as not containing single cells that actually contained single cells[45]. Precision = 1 means that all microwells scored as containing single cells actually contained

single cells. Sensitivity = 1 means that all microwells actually containing single cells were scored as containing single-cells. Precision and sensitivity metrics were 0.90 ± 0.09 and 0.68 ± 0.17 respectively (± S.D., $n$ = 56 blocks of 420 microwells on 8 separate slides), reflecting stringent selection of single-cell microwells at the expense of the total number of microwells included in downstream analysis.

Fluorescence images from the GenePix scanner were registered using landmark correspondences in Fiji (http://fiji.sc/Fiji). A custom script extracted line profiles from grids of regions of interest (ROIs) from each fluorescence image. Line profiles were background subtracted using linear interpolation between points set to the approximate boundaries of peaks of interest. Data quality control was performed by manually reviewing separation ROIs flagged due to outlying line profiles. Separations that were clearly affected by the presence of e.g. autofluorescent particulates were discarded from data sets, as were zero cell/microwell separations incorrectly scored as single-cell separations that did not contain β-tubulin loading control signals above technical noise.

Total areas under peaks (AUCs) of interest (or metrics derived from them, such as AUC ratios and calibrated AUCs) were transformed, where applicable, using the function $AUC_t = \text{arcsinh}(AUC/F)$, where $AUC_t$ is the arcsinh-transformed value and $F$ is a cofactor prescribing the transition from linear to log-like behavior. The value of $F$ was optimized by setting it according to $F = \mu_{ones,below} + 3\sigma_{ones,below}$, where $\mu_{ones,below}$ and $\sigma_{ones,below}$ are the mean and standard deviation of the set of single cell/microwell separations with fluorescence AUCs (or metrics) below a technical noise threshold. The technical noise threshold $T$ was set at $T = \mu_{zeros} + 3\sigma_{zeros}$, where $\mu_{zeros}$ and $\sigma_{zeros}$ are the mean and standard deviation of the AUCs or metric values from zero cell/microwell separations in a given experiment. Where applicable, separations with AUCs in the numerator of ratio metrics falling below $T$ were flagged to display as such when plotted. Separations with AUCs below $T$ in the denominator were discarded from data sets.

## Statistical analysis

Non-parametric comparison of scWestern data (single comparisons only) was performed using the Mann-Whitney U test in conjunction with Shapiro-Wilk and Levine tests for normality and equality of variance, respectively, in SPSS v.21 software (IBM).

## scWestern calibration

A conceptual overview and schematics of direct and indirect calibration assays are provided in Supplementary Note 6 and Supplementary Fig. 14. For “direct” calibration of EGFP, an 8-aliquot dilution series (40 μl per aliquot) of EGFP in denaturing RIPA buffer supplemented with 4 μM BSA (approximating total protein levels in single-cell separations) was added to distinct microwells of scWestern slides in the ArrayIt hybridization cassette (Supplementary Fig. 15). Slides were sandwiched and assayed as for purified protein assays (see **Purified protein scWesterns**.) with one additional step. A subset of microwells in each block were imaged for EGFP fluorescence (10× magnification, 200 ms exposure time, 1×1 pixel binning) immediately prior to the electrophoresis step using a preset position list to guide the mechanical stage on the IX71 fluorescence microscope. Partition coefficients

across the concentration range were determined from these images according to $K = ([EGFP]_{gel} - [EGFP]_{gel,bg})/([EGFP]_{microwell} - [EGFP]_{microwell,bg})$, where $[EGFP]_{gel}$ and $[EGFP]_{microwell}$ are in-gel and in-microwell concentrations of EGFP at equilibrium determined by fluorescence calibration in a separate microfluidic channel of 30 μm depth (Supplementary Fig. 4). Custom straight-channel microfluidic chips were fabricated in soda lime glass using standard wet-etching processes (PerkinElmer). $[EGFP]_{gel,bg}$ and $[EGFP]_{microwell,bg}$ correct for the background fluorescence of the scWestern slide prior to incubation with the EGFP solutions. The number of molecules of EGFP in each microwell voxel was also estimated from these data, assuming cylindrical microwells of nominal dimensions: 20 μm diameter, 30 μm depth (9.4 pl volume).

"Indirect" calibration was performed by capturing to the scWestern gel and probing a dilution series of a given purified protein in denaturing RIPA supplemented with 4 μM BSA in the absence of an electrophoresis step (Supplementary Fig. 14 and 15). Spot UV exposures were applied to the underside of the slide within each microwell block via the 10× objective for 45 s each on the Olympus IX71 fluorescence microscope through a custom UV-longpass filter set (excitation 300–380 nm, emission >410 nm; XF1001, XF3097; Omega Optical) with a UV power at the slide surface of ~40 $mW/cm^2$ (320–400 nm UV meter; C6080-365, Hamamatsu). The in-gel concentrations of purified proteins captured in this manner were determined from separate partition coefficient measurements using Alexa Fluor 568-labeled aliquots of each protein (Supplementary Fig. 4). Indirect calibration of EGFP reports molecule number using the inferred in-gel concentrations for a voxel size equivalent to that of a typical probed EGFP band from an scWestern experiment (45×45 μm in area, 30 μm in depth). Probe AFU and SNR values in indirect calibration data were corrected for fluorescence background caused by non-specific probing of UV-exposed gel spots in the absence of calibration standard.

### Integration of scWestern analysis with FACS

Live EGFP NSCs were sorted using an Influx v7 Sorter (BD Biosciences). BD FACS Sortware 1.0.0.650 was used to establish a 4×16 grid over the surface of a dried scWestern slide for deposition of sorted cells. 10 μm polystyrene fluorescent microspheres (Flow-Check Fluorospheres, 6605359, Beckman Coulter) were test-sorted for fine positioning adjustment. Cells were gated for EGFP expression, and sorting was calibrated so that each droplet exiting the nozzle contained a single EGFP-positive cell or no cells. The sorting purity was ~96%. After FACS, gel slides were rehydrated by immersion in PBS and analyzed by scWestern. For propidium iodide (PI) cell staining, PI (1mg/mL, P3566, Life Technologies) was added to cell suspensions at 1:100 dilution. Dead cells were imaged after drying of FACS droplets on scWestern slides by fluorescence microscopy.

### Determination of bulk buffer velocity during in-microwell lysis

Bulk maximum flow speeds during lysis (ignoring vector information) were estimated by widefield fluorescence microscopy (4× objective, EGFP filter set) during pouring of a 15 μm fluorescent microsphere-spiked RIPA buffer over a scWestern slide ($10^5$ microspheres/ml) at an exposure time of 10 ms (Supplementary Fig. 3). Velocities were extracted from fluorescence streaks caused by movement of microspheres in the horizontal plane over the

exposure period, with the objective focused ~1 mm above the center of the scWestern slide plane to observe bulk fluid behavior.

### COMSOL fluid modeling

Fluid flow in *sc*Westerm microwells was modeled in COMSOL Multiphysics 4.2a (Supplementary Note 1, Supplementary Fig. 3). Bulk flow above microwells was simulated as steady-state laminar flow of water in a square channel of crossection 100 × 100 μm. The top and side walls of the channel were set to a slip boundary condition. The bottom wall of the channel and the microwell walls were set to no-slip. Inlet velocity was set to 0.0087 m/s to achieve a maximum bulk flow velocity of 0.013 m/s. Outlet pressure was set to 0. Microwell recirculation flow was visualized by the particle tracing module in COMSOL.

### Flow cytometry

For flow cytometry for EGFP expression; EGFP NSCs and uninfected NSCs were detached with accutase, fixed by suspension in 4% paraformaldehyde (P6148, Sigma-Aldrich) for 15 minutes, and then blocked and permeabilized with flow staining buffer (5% donkey serum with 1 mg/mL saponin; D9663 and 47036, Sigma-Aldrich; in PBS) for 15 minutes. Cells were incubated with goat anti-GFP (1:100; see **scWestern probing, imaging, and stripping**. for product details) in flow staining buffer for 1 hour; followed by incubation with Alexa Fluor 555-labeled donkey anti-goat IgG (1:100) in flow staining buffer for 1 hour. Cells were washed twice for 5 min each with staining buffer between application of primary and secondary antibodies, and finally for 5 min with staining buffer and twice for 5 min each with PBS immediately prior to performing flow analysis. Flow cytometry was performed using an EMD Millipore EasyCyte 6HT-2L.

### Conventional western blotting

For the signaling study in Fig. 3c, EGFP NSCs were seeded at $2.5 \times 10^5$ cells per well in a 6-well culture plate. Cells were FGF-starved for 16 hours, incubated with 20 ng/mL FGF-2 for the desired stimulation time, and lysed in RIPA buffer (50 mM tris, 150 mM NaCl, 1% NP-40, 0.5% sodium deoxycholate, 0.1% SDS, p*H* 8) containing protease and phosphatase inhibitor cocktails (87786 and 78420, ThermoFisher Scientific) and 10 mg/mL PMSF (78830, Sigma-Aldrich). For the differentiation assay in Fig. 4e, EGFP NSCs were seeded at $5 \times 10^5$ cells per dish in 6 cm dishes. Day 0 differentiated cells were lysed the following day; day 6 differentiated cells were cultured in differentiation media (DMEM-F12-N2, 0.5 ng/mL FGF-2, 1 μM RA, 1% FBS) for 6 days and then lysed. Cell lysates of equal total protein concentrations determined by a bicinchoninic acid assay (23227, ThermoFisher Scientific) were mixed with 5× Laemmli buffer (final 50mM Tris, 2% SDS, 0.1% Bromophenol Blue, 10% glycerol), 2-mercaptoethanol was added to 10% v/v, and samples were boiled at 95°C for 5 minutes. Samples were electrophoretically separated on SDS-PAGE gels of between 6 and 10%T and transferred onto nitrocellulose membranes using standard methods. Blots were blocked for 1 hour in TBST and 3% BSA for phoshoprotein antibodies or 5% non-fat powdered milk (6250, EMD Millipore) for all other antibodies. Blots were probed overnight with primary antibodies in the same blocking buffer: rabbit anti-pERK1/2 (1:2,000; see **scWestern probing, imaging, and stripping**. for product

details), rabbit anti-ERK1/2 (1:1,000), mouse anti-ERK1/2 (“ERK #2”, 1:1,000), mouse anti-MASH1 (1:1,000), mouse anti-SRC (1:1,000), goat anti-EphB4 (1:1,000), goat anti-GFP (1:1,000), rabbit anti-pMEK1/2 (1:1,000), rabbit anti-MEK1/2 (1:1,000), goat anti-SOX2 (1:500), mouse anti-nestin (1:1,000), mouse anti-nestin (“NEST #2”, clone: rat-401, 1:2,000), goat anti-GFAP (1:1,000), mouse anti-βIII-tubulin (1:2,000), rabbit anti-β-tubulin (1:500); followed by 1 hour incubation with appropriate horseradish peroxidase-conjugated secondary antibodies: mouse anti-goat HRP (1:5,000, 31400), goat anti-mouse HRP (1:10,000, 32430), goat anti-rabbit HRP (1:10,000, 32460), all from ThermoFisher Scientific. Protein bands were detected using SuperSignal West Dura Chemiluminescent Substrate (34076, ThermoFisher Scientific) and blots were digitally imaged on a ChemiDoc XRS+ Imaging System (BioRad). Blots were stripped in a solution of 3% acetic acid, 0.5M NaCl, pH 2.5 for 10 minutes, neutralized with 0.5M NaOH for 1 minute, and then re-probed as needed. Blot densitometry was performed in ImageJ by measuring background-subtracted ROI intensities.

For purified protein samples (Supplementary Fig. 6), 1 μg of Alexa Fluor 488-labeled OVA and/or 1 μg Alexa Fluor 488-labeled BSA were incubated in denaturing or standard RIPA buffer for 30 minutes at room temperature, protected from light. Samples were then mixed with 5× Laemmli buffer. For reducing conditions, 2-mercaptoethanol was added to samples to 10% v/v. For boiling conditions, samples were boiled at 95°C for 5 minutes; non-boiled samples were incubated at room temperature for 5 minutes. All samples were electrophoretically separated on a 10% SDS-PAGE gel. Fluorescent protein bands were directly imaged in-gel via the ChemiDoc instrument.

### Immunocytochemistry

For the signaling study in Fig. 3f, EGFP NSCs were seeded at $5 \times 10^3$ cells per well in a 96-well plate. Cells were FGF-starved and stimulated as described for conventional western blotting. For the differentiation assay in standard cell culture conditions (Fig. 4a), EGFP NSCs were seeded at $4 \times 10^4$ cells per well in a 24-well plate and differentiated. For scWestern microwells, EGFP NSCs were differentiated in culture plates, suspended on the appropriate day, settled into scWestern slides, and processed within ArrayIt hybridization cassettes. Cell cultures and settled cells were fixed with 4% paraformaldehyde for 15 minutes, and then blocked and permeabilized with staining buffer (5% donkey serum with 0.3% Triton-X100 in PBS) for 30 minutes. Cultures and cells were incubated 24–48 hours with combinations of primary antibodies in staining buffer: rabbit anti-pERK1/2 (1:200; see **scWestern probing, imaging, and stripping**. for product details), mouse anti-ERK1/2 (1:50, 4696, Cell Signaling), rabbit anti-pMEK1/2 (1:200), mouse anti-MEK1/2 (1:25, 4694, Cell Signaling), goat anti-SOX2 (1:100), mouse anti-nestin (1:200), goat anti-GFAP (1:500), mouse anti-βIII-tubulin (1:500); followed by 2 hour incubations with appropriate Cy3-, Alexa Fluor 555-, and 647-labeled donkey anti-mouse, rabbit, or goat IgG secondary antibodies (1:250, Life Technologies; 15-165-150, 715-605-150, 711-605-152, 705-605-147, Jackson ImmunoResearch), with DAPI as a nuclear counterstain (5 μg/mL, D1306, Life Technologies). Cell cultures were imaged using a Nikon Eclipse T*i* inverted fluorescence microscope (Nikon Instruments) or an ImageXpress Micro XL Widefield High

Content Screening System (Molecular Devices). In-microwell cells were imaged using the Olympus IX71 microscope (see **scWestern**.).

Confocal images were obtained on a BX51W1 microscope (Olympus) with swept-field confocal optics (Prairie Technologies) and analyzed with Icy bioinformatics software (http://icy.bioimageanalysis.org). For confocal imaging of differentiated cells in scWestern microwells in Fig. 4c, rabbit anti-GFAP (1:500, ab7260, Abcam) was used; all other antibody reagents were identical to those listed.

### Immunocytochemistry data analysis

For the signaling study in Fig. 3f, cells were identified via custom ImageJ scripts using thresholding and particle analysis to locate DAPI-stained nuclei. Single cells for analysis were isolated and selected by gating for distance to nearest neighbor cells and uniformity of background signal in R. Fluorescence was quantified by summing pixel intensities of a background-subtracted 75 × 75 pixel ROI around each single cell. Approximately 50% of pixels in each ROI consisted of background signal, which was Gaussian in distribution. The intensity value with highest pixel count was taken to be the mean background intensity and used for background subtraction for individual ROIs. A noise threshold was set to $T = 3\sigma_{bg}$, where $\sigma_{bg}$ is the maximum standard deviation of background signal intensity in the fluorescence micrographs at each experimental condition. Measurements with fluorescence below $T$ in the numerator were identified as such in plotted data. Measurements with fluorescence below $T$ in the denominator were discarded from data sets.

Fluorescence micrographs from ICC experiments in culture plates and scWestern microwells for the differentiation experiment in Fig. 4a,b were manually scored for marker expression according to arbitrarily determined fluorescence thresholds in ImageJ. Different, blinded researchers conducted ICC counting and scWestern marker expression analyses.

## Supplementary Material

Refer to Web version on PubMed Central for supplementary material.

## ACKNOWLEDGEMENTS

We acknowledge E. Connelly for assistance with cell culture and conventional western blots, K. Heydari at the UC Berkeley Cancer Research Laboratory Flow Cytometry Facility for assistance with interfacing with FACS; R. Lin, L. Bugaj, E. Woods, and C. Nilson for critical discussion; and the QB3 Biomolecular Nanotechnology Center (BNC) at UC Berkeley for partial infrastructure support. A.J.H. is a 2013 Siebel Scholar. D.P.S. is a 2014 Siebel Scholar and was supported by a California Institute for Regenerative Medicine training grant. A.E.H. is an Alfred P. Sloan Research Fellow in chemistry. This work was supported by a U.S. National Institutes of Health (NIH) New Innovator Award (DP2OD007294 to A.E.H.), a Medical Research Program Grant from the W.M. Keck Foundation (to A.E.H.), a UC Berkeley Bakar Fellowship (to A.E.H); and a U.S. NIH research project grant (R01ES020903 to D.V.S).

## REFERENCES

1. Altschuler SJ, Wu LF. Cellular heterogeneity: Do differences make a difference? Cell. 2010; 141:559–563. [PubMed: 20478246]
2. Chang HH, Hemberg M, Barahona M, Ingber DE, Huang S. Transcriptome-wide noise controls lineage choice in mammalian progenitor cells. Nature. 2008; 453:544–547. [PubMed: 18497826]

3. Raj A, Rifkin SA, Andersen E, van Oudenaarden A. Variability in gene expression underlies incomplete penetrance. Nature. 2010; 463:913–918. [PubMed: 20164922]
4. Dalerba P, et al. Single-cell dissection of transcriptional heterogeneity in human colon tumors. Nat Biotechnol. 2011; 29:1120–1127. [PubMed: 22081019]
5. Balic M, Williams A, Lin H, Datar R, Cote RJ. Circulating tumor cells: From bench to bedside. Annu Rev Med. 2013; 64:31–44. [PubMed: 23092385]
6. Lazzara MJ, et al. Impaired SHP2-mediated extracellular signal-regulated kinase activation contributes to gefitinib sensitivity of lung cancer cells with epidermal growth factor receptor-activating mutations. Cancer Res. 2010; 70:3843–3850. [PubMed: 20406974]
7. Bendall SC, et al. Single-cell mass cytometry of differential immune and drug responses across a human hematopoietic continuum. Science. 2011; 332:687–696. [PubMed: 21551058]
8. Zong C, Lu S, Chapman AR, Xie XS. Genome-wide detection of single-nucleotide and copy-number variations of a single human cell. Science. 2012; 338:1622–1626. [PubMed: 23258894]
9. Taniguchi Y, et al. Quantifying E. coli proteome and transcriptome with single-molecule sensitivity in single cells. Science. 2010; 329:533–538. [PubMed: 20671182]
10. Schwanhausser B, et al. Global quantification of mammalian gene expression control. Nature. 2011; 473:337–342. [PubMed: 21593866]
11. Newman JRS, et al. Single-cell proteomic analysis of S. cerevisiae reveals the architecture of biological noise. Nature. 2006; 441:840–846. [PubMed: 16699522]
12. Wei W, et al. Microchip platforms for multiplex single-cell functional proteomics with applications to immunology and cancer research. Genome Med. 2013; 5
13. Ashton RS, et al. Astrocytes regulate adult hippocampal neurogenesis through ephrin-B signaling. Nat Neurosci. 2012; 15:1399–1406. [PubMed: 22983209]
14. Sevecka M, MacBeath G. State-based discovery: A multidimensional screen for small-molecule modulators of EGF signaling. Nat Methods. 2006; 3:825–831. [PubMed: 16990815]
15. Spurrier B, Ramalingam S, Nishizuka S. Reverse-phase protein lysate microarrays for cell signaling analysis. Nat Protoc. 2008; 3:1796–1808. [PubMed: 18974738]
16. Stadler C, et al. Immunofluorescence and fluorescent-protein tagging show high correlation for protein localization in mammalian cells. Nat Methods. 2013; 10:315–323. [PubMed: 23435261]
17. Maecker HT, Trotter J. Flow cytometry controls, instrument setup, and the determination of positivity. Cytom Part A. 2006; 69A:1037–1042.
18. Schulz KR, Danna EA, Krutzik PO, Nolan GP. Single-cell phospho-protein analysis by flow cytometry. Curr Protoc Immunol. 2012; 96:8.17.11–18.17.20.
19. Towbin H, Staehelin T, Gordon J. Electrophoretic transfer of proteins from polyacrylamide gels to nitrocellulose sheets: Procedure and some applications. Proc Natl Acad Sci USA. 1979; 76:4350–4354. [PubMed: 388439]
20. Ciaccio MF, Wagner JP, Chuu CP, Lauffenburger DA, Jones RB. Systems analysis of EGF receptor signaling dynamics with microwestern arrays. Nat Methods. 2010; 7:148–155. [PubMed: 20101245]
21. Hughes AJ, Herr AE. Microfluidic western blotting. Proc Natl Acad Sci USA. 2012; 109:21450–21455. [PubMed: 23223527]
22. Shapiro AL, Vinuela E, Maizel JV. Molecular weight estimation of polypeptide chains by electrophoresis in SDS-polyacrylamide gels. Biochem Biophys Res Commun. 1967; 28:815–820. [PubMed: 4861258]
23. Gallagher S, Winston SE, Fuller SA, Hurrell JG. Immunoblotting and immunodetection. Curr Protoc Immunol. 2008; 8.10
24. Friedman N, Cai L, Xie XS. Linking stochastic dynamics to population distribution: An analytical framework of gene expression. Phys Rev Lett. 2006; 97:168–302.
25. Cai L, Friedman N, Xie XS. Stochastic protein expression in individual cells at the single molecule level. Nature. 2006; 440:358–362. [PubMed: 16541077]
26. Cohen AA, et al. Protein dynamics in individual human cells: Experiment and theory. PLoS ONE. 2009; 4:e4901. [PubMed: 19381343]

27. Bendall SC, Nolan GP, Roederer M, Chattopadhyay PK. A deep profiler's guide to cytometry. Trends Immunol. 2012; 33:323–332. [PubMed: 22476049]
28. Gage FH, et al. Survival and differentiation of adult neuronal progenitor cells transplanted to the adult brain. Proc Natl Acad Sci USA. 1995; 92:11879–11883. [PubMed: 8524867]
29. Peltier J, O'Neill A, Schaffer DV. PI3K/Akt and CREB regulate adult neural hippocampal progenitor proliferation and differentiation. Dev Neurobiol. 2007; 67:1348–1361. [PubMed: 17638387]
30. Jensen KJ, et al. An ERK-p38 subnetwork coordinates host cell apoptosis and necrosis during coxsackievirus b3 infection. Cell Host Microbe. 2013; 13:67–76. [PubMed: 23332156]
31. Huang CYF, Ferrell JE. Ultrasensitivity in the mitogen-activated protein kinase cascade. Proc Natl Acad Sci USA. 1996; 93:10078–10083. [PubMed: 8816754]
32. Eldar A, Elowitz MB. Functional roles for noise in genetic circuits. Nature. 2010; 467:167–173. [PubMed: 20829787]
33. Chou YH, Khuon S, Herrmann H, Goldman RD. Nestin promotes the phosphorylation-dependent disassembly of vimentin intermediate filaments during mitosis. Mol Biol Cell. 2003; 14:1468–1478. [PubMed: 12686602]
34. Hyder CL, Isoniemi KO, Torvaldson ES, Eriksson JE. Insights into intermediate filament regulation from development to ageing. J Cell Sci. 2011; 124:1363–1372. [PubMed: 21502133]
35. Sahlgren CM, et al. Mitotic reorganization of the intermediate filament protein nestin involves phosphorylation by cdc2 kinase. JBC. 2001; 276:16456–16463.
36. Yang HY, Lieska N, Goldman AE, Goldman RD. Colchicine-sensitive and colchicine-insensitive intermediate filament systems distinguished by a new intermediate filament-associated protein, IFAP-70/280kD. Cell Motil Cytoskel. 1992; 22:185–199.
37. Su PH, et al. Identification and cytoprotective function of a novel nestin isoform, Nes-S, in dorsal root ganglia neurons. JBC. 2013; 288:8391–8404.
38. Hendrickson ML, Rao AJ, Demerdash ONA, Kalil RE. Expression of nestin by neural cells in the adult rat and human brain. PLoS ONE. 2011; 6:e18535. [PubMed: 21490921]
39. Marx V. Finding the right antibody for the job. Nat Methods. 2013; 10:703–707.
40. Fujioka A, et al. Dynamics of the Ras/ERK MAPK cascade as monitored by fluorescent probes. JBC. 2006; 281:8917–8926.

## METHODS REFERENCES

41. Yu JH, Schaffer DV. Selection of novel vesicular stomatitis virus glycoprotein variants from a peptide insertion library for enhanced purification of retroviral and lentiviral vectors. J Virol. 2006; 80:3285–3292. [PubMed: 16537595]
42. Peltier J, Schaffer DV. Viral packaging and transduction of adult hippocampal neural progenitors. Methods Mol Biol. 2010; 621:103–116. [PubMed: 20405362]
43. Hughes AJ, Lin RKC, Peehl DM, Herr AE. Microfluidic integration for automated targeted proteomic assays. Proc Natl Acad Sci USA. 2012; 109:5972–5977. [PubMed: 22474344]
44. Hughes AJ, Herr AE. Quantitative enzyme activity determination with zeptomole sensitivity by microfluidic gradient-gel zymography. Anal Chem. 2010; 82:3803–3811. [PubMed: 20353191]
45. Selinummi J, et al. Bright field microscopy as an alternative to whole cell fluorescence in automated analysis of macrophage images. PLoS ONE. 2009; 4:e7497. [PubMed: 19847301]

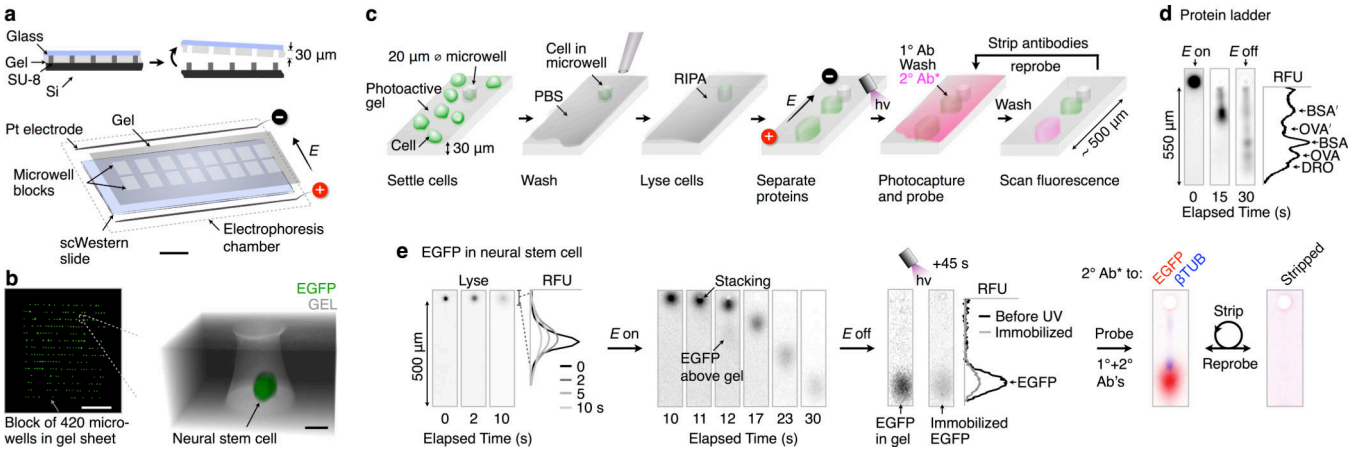


**Figure 1.**

Single-cell western blotting. (**a**) The scWestern array consists of thousands of microwells (20 µm diameter, 30 µm deep) patterned in a 30 µm-thick photoactive polyacrylamide gel seated on a glass microscope slide. The array is comprised of 16 blocks of 14×30 microwells (6,720 in total) cast against an SU-8 photoresist master fabricated by soft lithography. E: electric field. Scale bar: 10 mm. (**b**) Widefield micrograph of a microwell block containing 15 µm fluorescent microspheres (scale bar: 2 mm), and confocal micrograph of a live EGFP-expressing neural stem cell (NSC) settled in a rhodamine-tagged gel (GEL, scale bar: 10 µm). (**c**) Open-gel scWestern analysis is a 4 hour, 6 stage assay comprised of: cell settling, chemical lysis with a denaturing RIPA buffer, polyacrylamide gel electrophoresis (PAGE), UV-initiated protein immobilization onto the gel (hν: photon energy), diffusion-driven antibody probing (i.e., primary and fluorescently-labeled secondary antibody probes; 1° Ab and 2° Ab*), and fluorescence imaging. (**d**) PAGE resolves 5 fluorescently labeled proteins in a 550 µm separation distance (DRO, dronpa 27 kDa; OVA, ovalbumin 45 kDa; BSA, bovine serum albumin 66 kDa; OVA´, OVA dimer 90 kDa; BSA´, BSA dimer 132 kDa). (**e**) scWestern analysis of EGFP and β-tubulin (βTUB) from a single NSC (RFU: relative fluorescence units). Distinct fluorescent dyes on each secondary antibody enable multiplexed target analysis (EGFP: Alexa Fluor 488-labeled secondary antibody, βTUB: Alexa Fluor 555−). Chemical stripping and re-probing allows multiplexed scWestern analysis. Antibody details for all figures are in **Online Methods**.

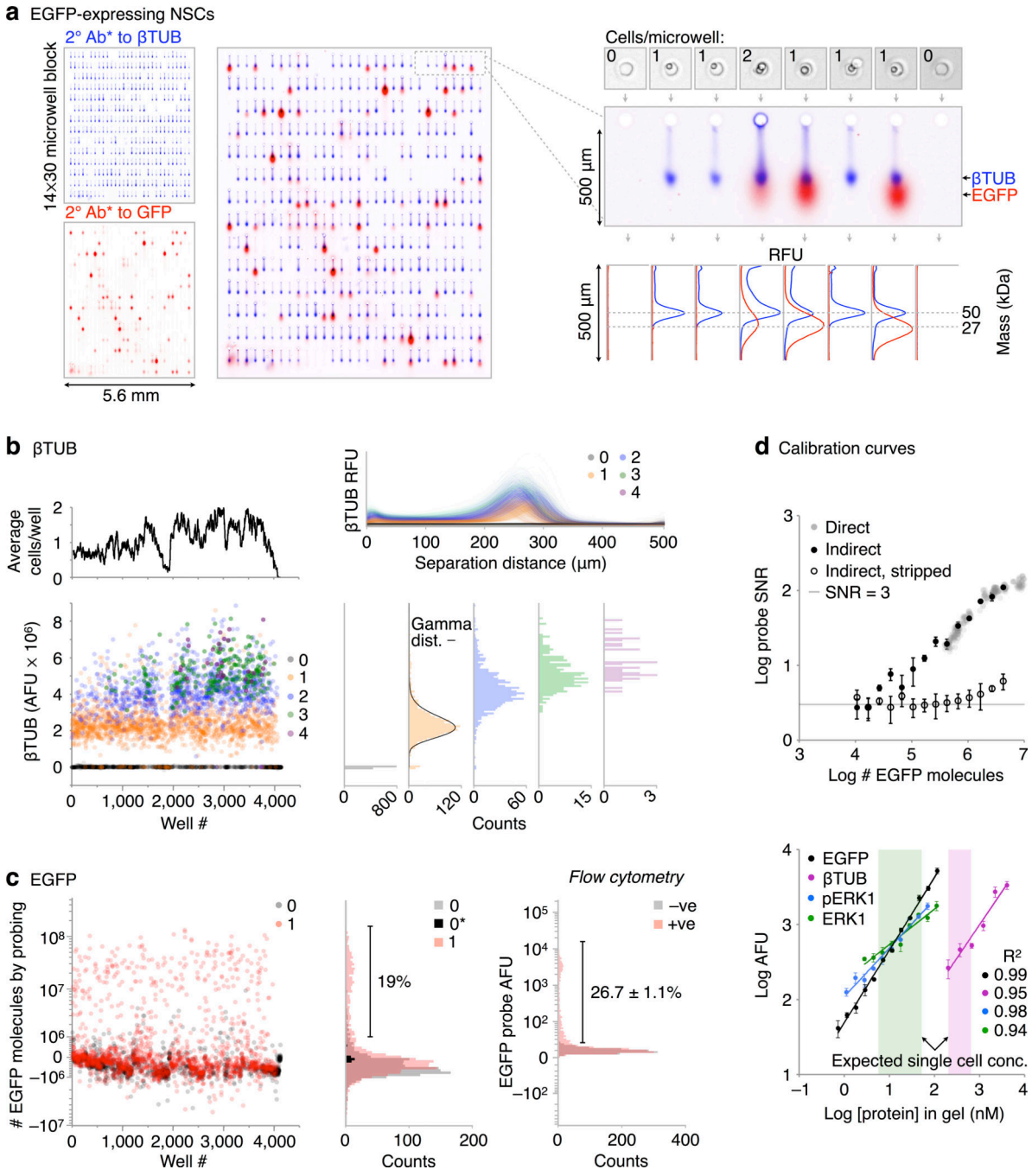


**Figure 2.**

scWestern blotting of NSCs. (**a**) 420 concurrent scWesterns of EGFP-expressing NSCs for βTUB (Alexa Fluor 647-labeled secondary antibody, 2° Ab*) and EGFP (Alexa Fluor 555−). Bright-field imaging determines cells/microwell. (**b**) Top-right: scWestern fluorescence for 4,128 separations by cells/microwell. Bottom-left: area under the curve for βTUB with (above) running average of cells/microwell (window size = 30 microwells). Microwells indexed from left-hand to right-hand side of array. Bottom-right: Fit of fluorescence distribution for single cells to gamma distribution stemming from Poissonian

mRNA production and exponentially distributed protein burst sizes $f(x)=(x^{a-1}e^{-x/b})/(\Gamma(a)b^a)$; $x$ = total probed band fluorescence, $a = \mu_p^2/\sigma_p^2 = 14.8$, $b = \sigma_p^2/\mu_p = 1.6\times10^5$ AFU, $\mu_p$ = mean band fluorescence, $\sigma_p^2$ = variance in band fluorescence, $\Gamma$ is the gamma function. (**c**) EGFP fluorescence for 1 and 0 cell/microwell blots compared to flow cytometry of fixed NSCs (EGFP transfected, +ve; untransfected, −ve), note arcsinh-transformed scales (**Online Methods**). Technical noise estimated from scWesterns with 0 cell/microwell in a sparsely cell-seeded region (separations 4,100–4,128, 0*; Supplementary Note 5). Fraction EGFP+ cells is mean ± S.D. for $n = 3$. (**d**) Signal-to-noise estimates limit of detection at 27,000 molecules using purified EGFP through direct and indirect methods (see text, mean ± S.D., $n = 3$ regions of interest per dot blot). Bottom, linear indirect calibration curves for purified standards (mean ± S.D., $n = 3$ regions of interest per dot blot) span physiologically relevant βTUB and ERK concentrations (concentration in a probed band estimated from in-cell concentrations[10,40]).

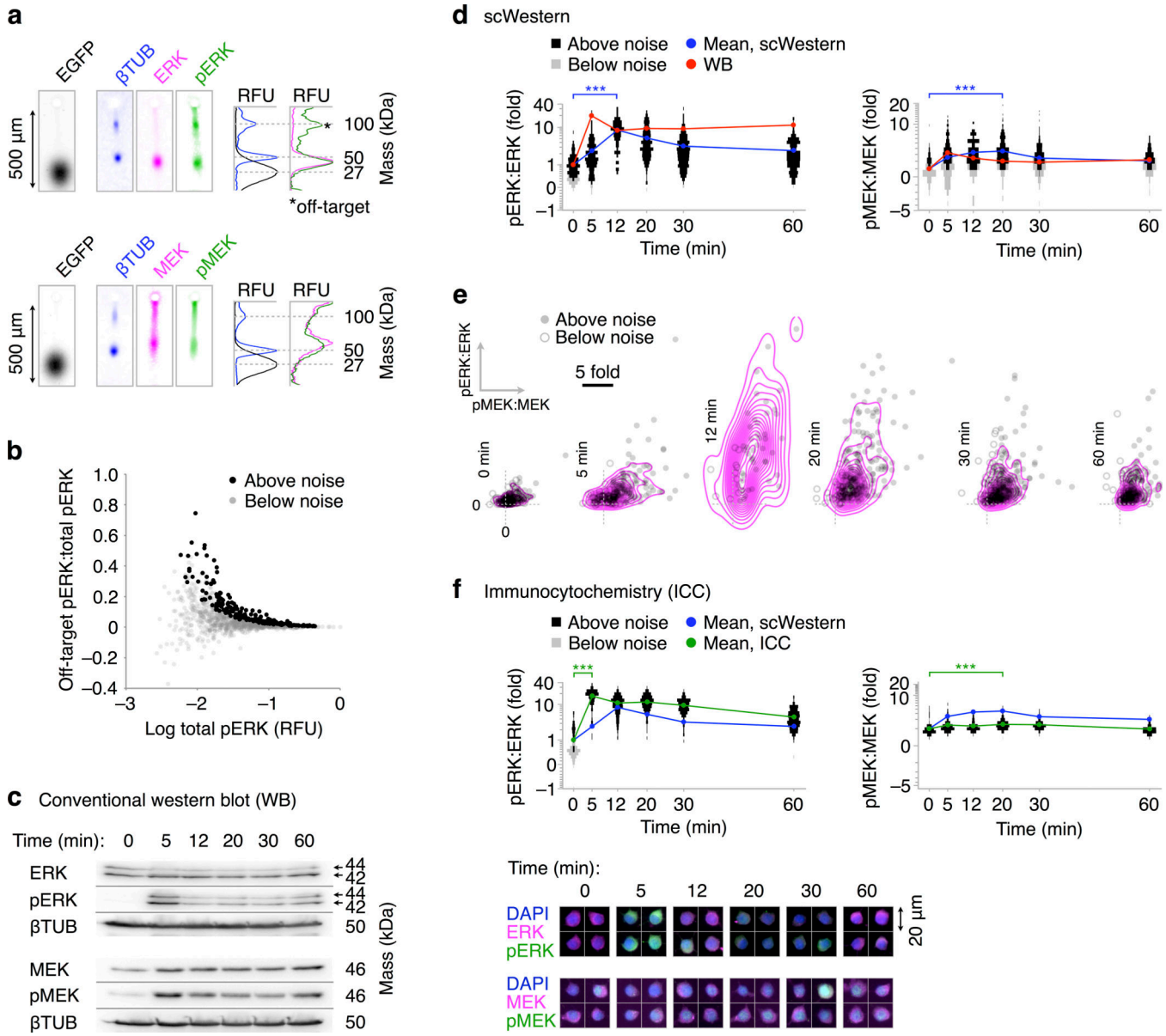


**Figure 3.**

scWesterns capture fibroblast growth factor-2 (FGF-2) signaling dynamics. (**a**) Fluorescence micrographs of scWesterns for ERK, pERK, MEK, pMEK in NSCs, with β-tubulin (βTUB) and EGFP ladder. For each target pair, EGFP image is from a distinct separation in the same microwell array row. 103 kDa off-target peak (via pERK antibody) does not coincide with ERK band. Secondary antibodies were Alexa Fluor 555-labeled (except EGFP; Alexa Fluor 488−) in order: pERK, ERK and EGFP co-probe, βTUB, pMEK, MEK; with stripping between probings. (**b**) Fraction off-target pERK versus total fluorescence for 1,117 scWesterns at timepoints from (**d**) and (**e**). (**c**) Conventional western blots (20 ng/ml FGF-2), cropped to show regions of interest. Full-length blots are presented in Supplementary Fig. 20. (**d**) Fold-change of pERK and pMEK to total ERK and MEK, respectively, with signals below technical noise indicated. Note arcsinh-transformed scales. Overlay from

conventional western blot densitometry. ***P < 0.001, Mann-Whitney. *n* = 186, 186, 57, 236, 278, and 208 scWesterns for 0, 5, 12, 20, 30, and 60 min time-points, respectively. (**e**) Fold-change from (**d**) with spatial density contours. (**f**) Immunocytochemistry co-probing for pERK-ERK and pMEK-MEK pairs; Alexa Fluor 555-labeled secondary phospho-antibodies and Alexa Fluor 647-labeled secondary total-antibodies. pERK:ERK: *n* = 160, 115, 186, 158, 172, and 197 cells for 0, 5, 12, 20, 30, and 60 min time-points, respectively. pMEK:MEK: *n* = 184, 216, 220, 223, 223, and 270 cells for 0, 5, 12, 20, 30, and 60 min time-points, respectively.

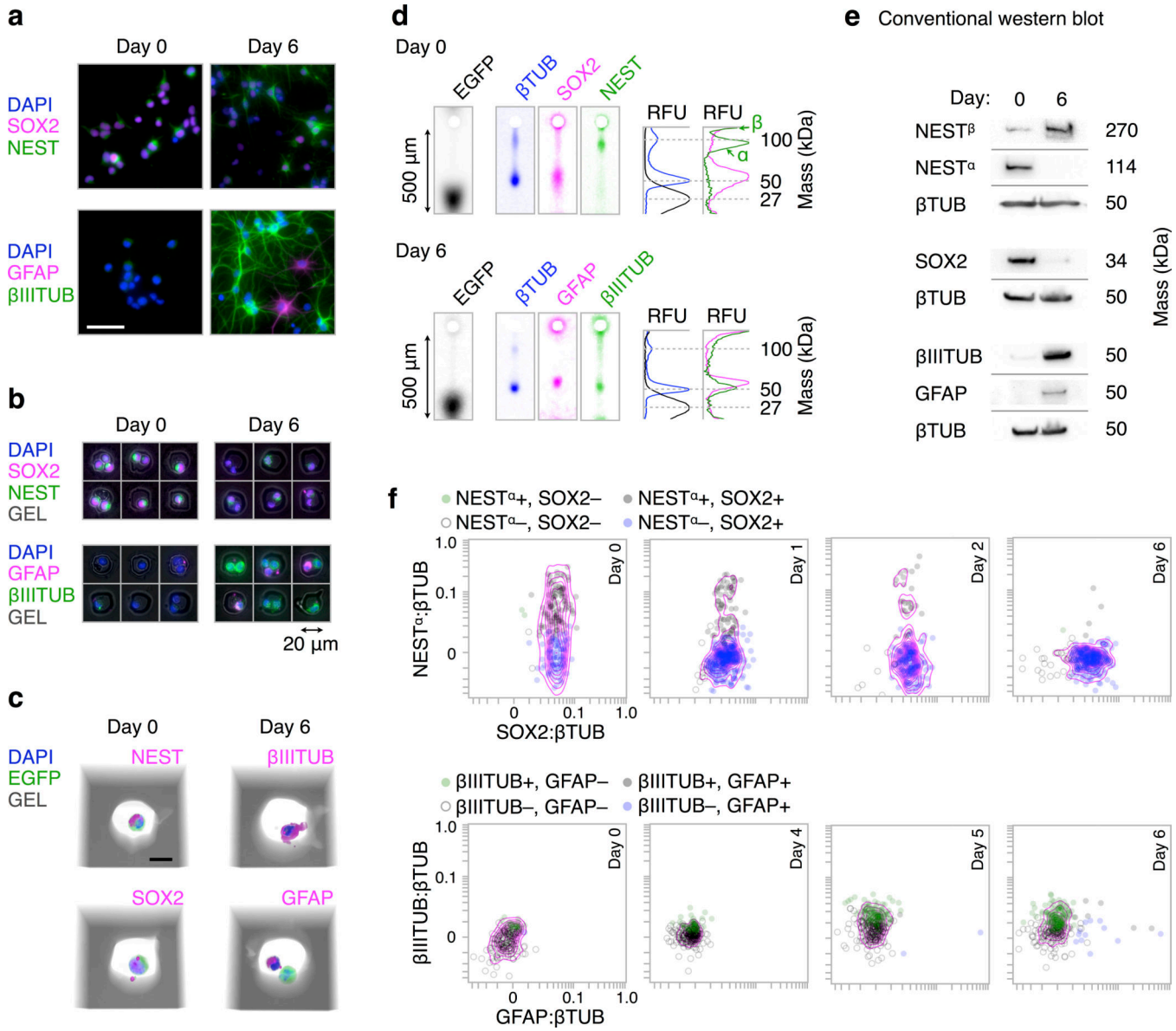


**Figure 4.**

scWesterns track NSC lineage commitment during differentiation. (**a**) Immunocytochemistry micrographs of mixed NSC differentiation cultures at days 0 and 6 for stem cell (nestin, NEST; SOX2) and differentiation markers (βIII-tubulin, βIIITUB; glial fibrillary acidic protein, GFAP). Scale bar: 50 μm. (**b**) Micrographs of NSCs in scWestern microwells, fixed and stained as in (**a**). (**c**) Confocal images of fixed and stained stem (NEST+, SOX2+), neuron (βIIITUB+) and astrocyte (GFAP+) cells in a rhodamine-tagged gel (GEL). Scale bar: 10 μm. (**d**) Inverted fluorescence micrographs of scWesterns. SOX2 (Alexa Fluor 555-labeled secondary antibody) and NEST (α and β isoforms, Alexa Fluor 488−) were co-probed in separate blocks as GFAP (Alexa Fluor 555−) and βIIITUB (Alexa Fluor 488−); both block sets were stripped and co-probed for β-tubulin (βTUB, Alexa Fluor 555−) and EGFP (Alexa Fluor 488−). Image sets from each day are the same separation, except EGFP images, which are from the same microwell array row as the corresponding

image set. (**e**) Cropped conventional western blots at differentiation days 0 and 6. Full-length blots are presented in Supplementary Fig. 29. (**f**) scWestern fluorescence normalized by βTUB (arbitrary units). Note arcsinh-transformed scales. Spatial density indicated by contours. scWestern blot NSC marker sample sizes, $n$ = 189, 353, 175, and 274 for time-points at 0, 1, 2, and 6 days, respectively. Differentiation marker sample sizes, $n$ = 178, 253, 303, 280 for time-points at 0, 4, 5, and 6 days, respectively. Data are one of two biological replicates performed.